Available online at www.sciencedirect.com
SCIENCE DIRECT®
International Journal of Thermal Sciences 42 (2003) 983–994
International Journal of Thermal Sciences
www.elsevier.com/locate/ijts

Constructal geometry and operation of adsorption processes

Alejandro Rivera-Alvarez [a], Adrian Bejan [b,*]

[a] *Energy and Thermodynamics Institute, Pontificia Bolivariana University, AA56006, Medellin, Colombia*
[b] *Department of Mechanical Engineering and Materials Science, Box 90300, Duke University, Durham, NC 27708-0300, USA*

Received 16 July 2002; accepted 17 February 2003

Abstract

This paper shows that the temporal and spatial structure of adsorption–desorption processes can be optimized for maximal packing of mass transfer into a fixed space, and for minimal overall pumping power. In the first part of the paper, simple models demonstrate that the periodicity of such processes can be optimized in three settings: fixed desorption time, variable desorption time, and variable species concentration in the gas space. The second part of the paper shows how the optimized time scales determine the dimensions of the smallest flow channels—the elemental system. The available space can be packed with elemental systems in a hierarchical (constructal) structure [Bejan, Shape and Structure, from Engineering to Nature, Cambridge University Press, 2000], in which elements are assembled into first constructs, first constructs are assembled into second constructs, etc. The robustness and nearly optimal performance of the optimized mass exchanger structure is discussed.

Keywords: Constructal; Adsorption; Optimization; Rhythm; Dendritic; Tree networks; Packing; Compactness; Mass exchangers; Fractal; Respiration

1. Introduction

In this paper we apply the constructal method [1] to the hierarchical multi-scale design of absorption systems with maximum "density" per unit volume and time. In all adsorption separation processes, the essential requirement is an adsorbent that adsorbs preferentially one component (or one family of related components) from a mixed feed. This selectivity may depend on a difference in adsorption equilibrium (equilibrium-selective) or on a difference in sorption rates (kinetically-selective) [2,3]. Adsorption separation processes involve two principal steps:

(i) adsorption, during which the preferentially adsorbed species are removed from the feed;
(ii) regeneration or desorption, during which these species are removed from the adsorbent, thus regenerating the adsorbent for use in the next cycle.

It is possible to obtain useful products from either the adsorption or desorption steps, or from both steps. The mechanism used in the desorption step differentiates the separation processes into two classes. When the removal is induced by reducing the pressure the process is called Pressure Swing Adsorption process (PSA). When it is induced by raising the temperature it is called Thermal Swing Adsorption process. Major applications of the kinetically adsorption processes are the production of nitrogen by air separation and separation of hydrocarbons from gas mixtures [3].

The intermittent nature of the adsorption processes makes it suitable for optimization of the times involved. In equilibrium-selective processes, however, cycle times are not the direct variable to control, because equilibrium is reached almost instantly and mass transfer rates are not so important [4]. Instead, the variables that are more suitable for optimization refer to flow rates and geometrical features [5]. In kinetically-selective processes, the cycle times are the variables to control, because mass transfer rates are most important [6].

Optimization of the cycle times can be carried out in order to select several variables. For example, one can adjust the pressurization and depressurization times to obtain a product with maximum purity, or the maximum amount of product per unit time, or production with minimum cost or

* Corresponding author.
E-mail address: dalford@duke.edu (A. Bejan).

1290-0729/$ – see front matter
doi:10.1016/S1290-0729(03)00077-2

Nomenclature

a	dimensionless adsorbed quantity	
$\bar{a}$	dimensionless time-averaged rate of A production	
A	area	m^2
C_A	concentration of species A in the solid adsorbent	$kmol \cdot m^{-3}$
C_{Ag}	concentration of species A in the gas	$kmol \cdot m^{-3}$
C_{As}	concentration of species A in the solid–gas surface	$kmol \cdot m^{-3}$
d	gas layer thickness	m
d	channel spacing	m
d_s	solid layer thickness	m
d_w	mechanical strength layer thickness	m
D	mass diffusivity of A in the gas mixture	$m^2 \cdot s^{-1}$
D_s	mass diffusivity of A in the solid	$m^2 \cdot s^{-1}$
j_A	mass flux of species A	$kmol \cdot m^{-2} \cdot s^{-1}$
$\bar{j}_A$	time-averaged mass flux of species A	$kmol \cdot m^{-2} \cdot s^{-1}$
K	Henry coefficient	
K_A	Henry coefficient of species A	
K_0	Henry coefficient at infinite temperature	
L	length	m
$\dot{m}'$	mass flow rate per unit length	$kg \cdot s^{-1} \cdot m^{-1}$
$\dot{m}''$	volumetric rate of gas flow	$kg \cdot m^{-3} \cdot s^{-1}$
n	number of stacked elements	
$\dot{n}$	volumetric rate of species removal	$kmol \cdot m^{-3} \cdot s^{-1}$
P	pressure	Pa
r	solid and gas layers thickness ratio	
R	universal gas constant	$J \cdot kmol^{-1} \cdot K^{-1}$
Sc	Schmidt number	
T	temperature	K
t	time	s
U	velocity of gas mixture	$m \cdot s^{-1}$
U_m	overall mass transfer coefficient	$m \cdot s^{-1}$
$\dot{W}'$	pumping power	$W \cdot m^{-1}$
$\widetilde{W}$	dimensionless pumping power	
y_A	molar fraction of species A	

Greek symbols

ΔC	concentration difference	$kmol \cdot m^{-3}$
ΔP	pressure drop	$N \cdot m^{-2}$
ΔP_L	pressure drop along channel	$N \cdot m^{-2}$
ΔU	activation energy	$J \cdot kmol^{-1}$
θ	dimensionless time	
μ	viscosity	$kg \cdot s^{-1} \cdot m^{-1}$
ν	kinematic viscosity	$m^2 \cdot s^{-1}$
ρ	density	$kg \cdot m^{-3}$
τ	desorption–adsorption times ratio	
ϕ	volume fraction occupied by flow channel	

Subscripts

0	initial
1	adsorption step, or first construct
2	desorption step, or second construct
3	third construct
a	adsorption
A	species A
B	species B
d	desorption
eq	equilibrium
f	final
max	maximum
opt	optimum
s	solid

minimum exergy destruction. Several publications describe the relationships between cycle times and product purity [6–8] and lost exergy [7].

In the first part of this paper we show that the time intervals of the production cycle can be optimized in order to achieve the maximum time-average rate of production. This class of optimal times adds to the list of engineered systems that have an optimized intermittent operation [1], and acquire structure in time. The time models are the simplest, and the results may seem trivial, but this is intentional. We want to show in the most basic sense that opportunities to optimize rhythm exist. In the second part of the paper we consider the spatial construction of a volume designed for maximum absorption *density*. As in maximum-compactness architectures for heat exchangers [9] and animal body insulation [10], the flow structure consists of two trees matched canopy to canopy. The smallest (elemental) volume scale with which the constructal sequence begins is dictated by the diffusion length associated with the optimized time scale optimized in the first part of the paper.

2. Fixed desorption time

In the following analysis we consider the simplest model that retains the main features of the process. Fig. 1 shows the system model. The following assumptions are made: there are two gaseous components (A and B), the process is modeled as 'open batch' (meaning that the length scale is omitted in the analysis; this is valid when $U_m/U \ll d/L$), the concentration of each component is constant in the gas, the equilibrium between gas and the solid–gas interface is dictated by Henry's law, and there is mass transfer from the solid–gas interface to the solid adsorbent for only one of the components (A), and the desorption time is fixed. These simplifying assumptions are discussed further in Section 9.

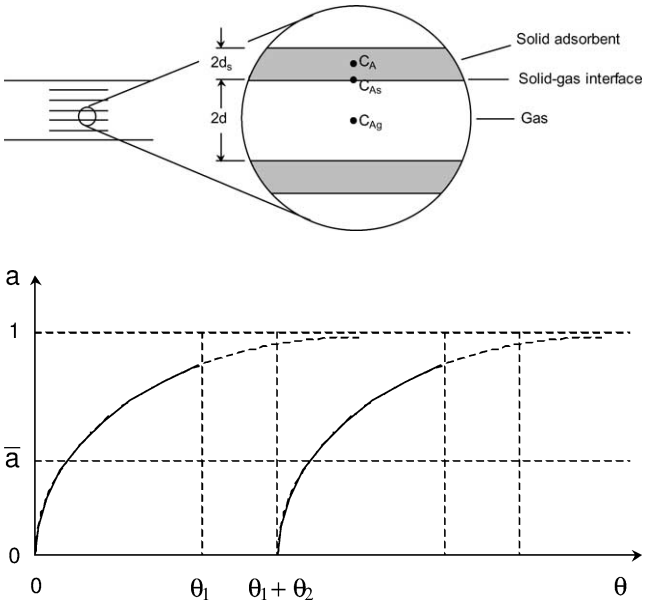

Fig. 1. Top: Channel filled with a gaseous mixture, and transversal adsorption of species A in the adsorbing wall. Bottom: Sequence of two adsorption (θ_1) – desorption (θ_2) cycles.

Adsorption proceeds in the direction perpendicular to the gas–solid interface, and is located at the surface.

As shown in Fig. 1, C_{Ag}, C_{As} and C_A are, respectively, the concentrations of species A in the gas, solid–gas interface (surface) and solid adsorbent. The mass balance for species A at the solid surface requires

$$\frac{\mathrm{d}C_A}{\mathrm{d}t} = \frac{U_m}{d_s}(C_{As} - C_A) \tag{1}$$

Here U_m is the global coefficient of mass transfer for the species A. It is assumed that only species A is adsorbed. In the adsorption step C_{As} is greater than C_A, and species A flows from gas to solid. In the desorption step C_{As} is smaller than C_A, and species A flows from solid to gas. The initial condition is

$$C_A = C_{A0} \quad \text{at } t = 0 \tag{2}$$

In the case of adsorption, C_{A0} represents the residual concentration in the preceding desorption step. When Eqs. (1) and (2) refer to desorption, C_{A0} represents the final concentration of the adsorption step. Henry's law provides a relationship between the gas and surface concentration

$$C_{As} = K_A C_{Ag} \tag{3}$$

where K_A is the Henry coefficient for the equilibrium solid–gas of species A. In this model, the concentration of A in the gas (C_{Ag}) is assumed constant. This assumption will be relaxed in Section 4.

The two-component gas is modeled as an ideal gas mixture, therefore C_{Ag} is given by

$$C_{Ag} = \frac{P_A}{RT} = \frac{y_A P}{RT} \tag{4}$$

where P_A, y_A, R, T and P are the partial pressure of component A, the molar fraction of component A, the universal gas constant, the temperature and the total pressure of the gas mixture. The concentration of A in the gas (C_{Ag}) can be changed by changing P (Pressure Swing Adsorption) or by changing T (Thermal Swing Adsorption). By solving Eqs. (1)–(3), we calculate the amount of adsorbed species A

$$a = 1 - \exp(-\theta) \tag{5}$$

where

$$a = \frac{C_A - C_{A0}}{K_A C_{Ag} - C_{A0}}, \qquad \theta = \frac{U_m}{d_s} t \tag{6}$$

The dimensionless adsorbed quantity (a) takes values between 0 and 1. The limit $a = 0$ means that the solid surface has not adsorbed yet, and the concentration of species A in the solid is at the residual concentration level C_{A0}. The other extreme, $a = 1$, means that solid has adsorbed all the A of which it is capable of adsorbing, i.e., the concentration of A in the solid is at the maximum level possible, C_{As}. The dimensionless time θ is unrestricted, and can take values higher or lower than 1.

In a complete optimization of the cycle, the adsorption and desorption processes are coupled and must be optimized together. For simplicity, in this section we model only the adsorption process. For the desorption process we assume that the time allocated to it is fixed, θ_2. The adsorption time is variable, θ_1. Even when the desorption mechanism is not specified, the time can be controlled as we show later in Eq. (18): a pair of times (θ_1, θ_2) can be obtained by selecting the proper a_0 for the desorption mechanism. The lower portion of Fig. 1 shows a sequence of two complete cycles. The time-averaged rate of A production, or the average flow of species A from the gas to the solid, is proportional to the dimensionless quantity

$$\bar{a} = \frac{a_1}{\theta_1 + \theta_2} = \frac{1 - \exp(-\theta_1)}{\theta_1 + \theta_2} = \frac{1 - \exp(-\theta_2 \tau)}{\theta_2(\tau + 1)} \tag{7}$$

where a_1 is the total amount of A adsorbed during θ_1, and τ is the time ratio

$$\tau = \frac{\theta_1}{\theta_2} \tag{8}$$

According to the first of Eqs. (6), $\bar{a}$ takes values in the 0–1 range, and is equal to

$$\bar{a} = \frac{\bar{j}_A}{j_{A,\max}} \tag{9}$$

where $\bar{j}_A$ is the time-averaged mass flux of the produced A,

$$\bar{j}_A = \frac{C_{A1} - C_{A0}}{t_1 + t_2} \tag{10}$$

and $j_{A,\max}$ is the maximum mass flux, which occurs at the start of the adsorption process, cf. Eq. (1),

$$j_{A,\max} = \frac{U_m}{d_s}(K_A C_{Ag} - C_{A0}) \tag{11}$$

The time of adsorption θ_1 can be selected such that $\bar{a}$ is maximum. Fig. 2 shows the variation of $\bar{a}$ with τ for several

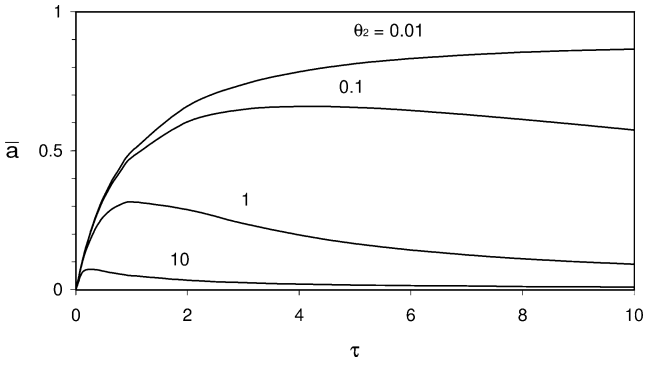

Fig. 2. The maximization of the time-averaged adsorption rate ($\bar{a}$) when the desorption time interval (θ_2) is fixed.

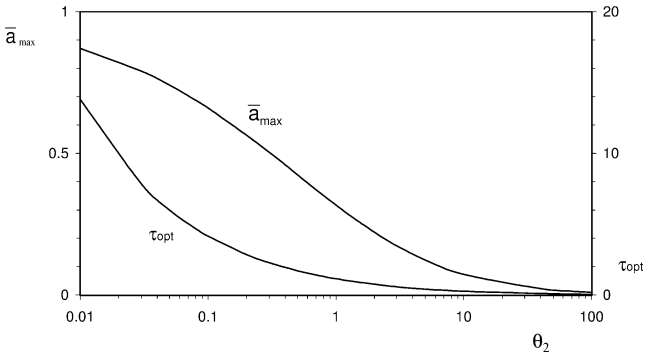

Fig. 3. The optimal time ratio and maximal average adsorption rate when the desorption process is not specified.

values of θ_2. There exists an optimal τ (or θ_1) for which the average rate of A production is maximum. The maximized production rate ($\bar{a}_{\max}$) is higher when θ_2 is shorter. By solving $\partial\bar{a}/\partial\tau = 0$ we determine the relation between τ_{opt} and θ_2,

$$1 + \theta_2(\tau_{\text{opt}} + 1) = \exp(\theta_2\tau_{\text{opt}}) \tag{12}$$

Combining this relation with Eq. (7) we obtain $\bar{a}_{\max}$ as a function of θ_2, as shown in Fig. 3. The same figure also shows τ_{opt} as a function of θ_2.

3. Variable desorption time

In the analysis presented in this section the constant-θ_2 assumption is not made. The desorption process consists of placing the solid in contact with a fluid of lower concentration of A. As shown in Fig. 4, during the two-stroke cycle two gaseous mixtures interact with the same solid, one mixture during adsorption ($\theta_1, C_{Aga} > C_A$), and another during desorption ($\theta_2, C_{Agd} < C_A$). We continue to assume that the concentrations of A at the surface are related to the concentrations in the gas through Henry's law,

$$C_{Asa} = K_{Aa}C_{Aga}, \qquad C_{Asd} = K_{Ad}C_{Agd} \tag{13}$$

Here K_{Aa} and K_{Ad} are the Henry constants for the adsorption and desorption steps, respectively.

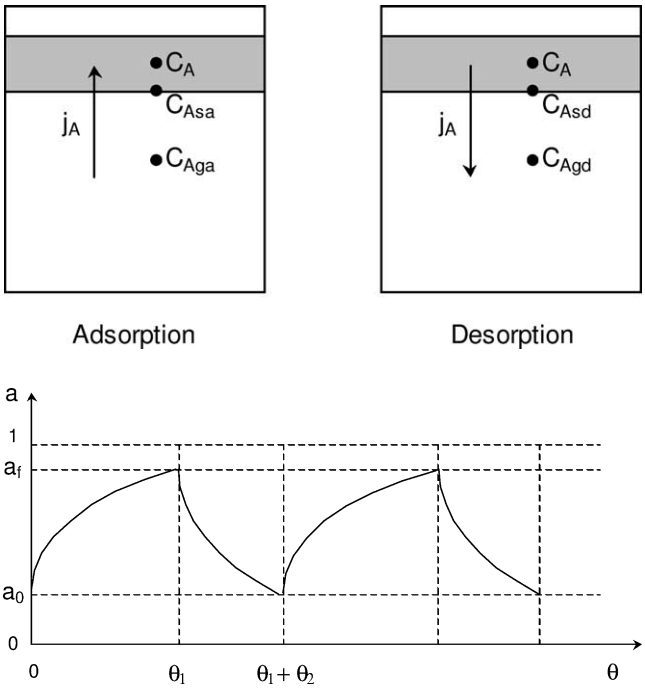

Fig. 4. Sequence of two adsorption–desorption cycles in which the two time intervals (θ_1, θ_2) may vary.

The concentration of A in the gas can be changed by changing the pressure or the temperature. When the pressure is changed, the Henry constants for adsorption and desorption are the same, $K_{Aa} = K_{Ad}$. When the temperature is changed, the Henry constants are related to the temperature through the van't Hoff relation

$$K = K_0 \exp(-\Delta U/RT) \tag{14}$$

where K, K_0, ΔU and R are the Henry constant, Henry constant at infinite temperature, activation energy, and universal gas constant. By solving Eqs. (1), (2) and (13) we obtain the amount of adsorbed species A during the adsorption step

$$a = 1 - (1 - a_0)\exp(-\theta) \tag{15}$$

This is equal to the amount of A removed during the desorption step

$$a = a_f \exp(-\theta) \tag{16}$$

where the dimensionless adsorbed quantity (a) takes values between 0 and 1

$$a = \frac{C_A - K_{Ad}C_{Agd}}{K_{Aa}C_{Aga} - K_{Ad}C_{Agd}} \tag{17}$$

The limit $a = 0$ means that the concentration of A in the solid is at the minimum level possible (C_{Asd}), i.e., equilibrium has been achieved with the gaseous mixture of the desorption step. The other extreme, $a = 1$, means that the concentration of A in the solid is at the maximum level possible (C_{Asa}), i.e., the solid is in equilibrium with the gaseous mixture of the adsorption step. The quantities a_0 and a_f refer to the final concentrations after the desorption

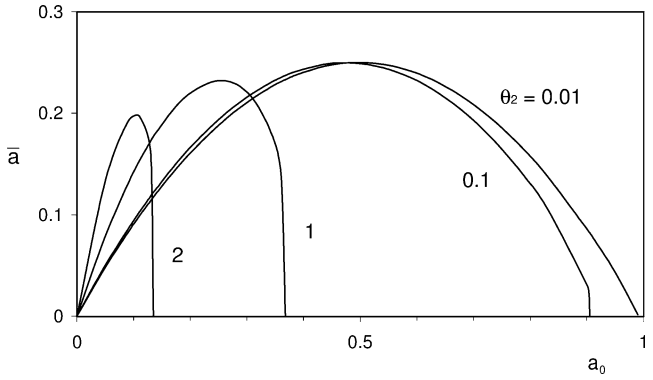

Fig. 5. The maximization of the averaged rate of species-A production, by varying a_0 at constant θ_2.

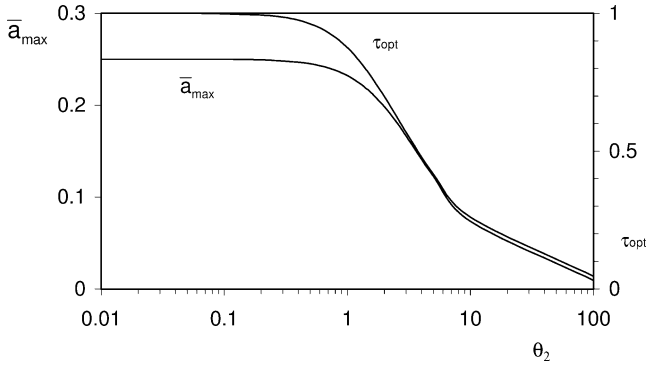

Fig. 6. The optimal time ratio and maximal average adsorption rate based on the model of Fig. 4.

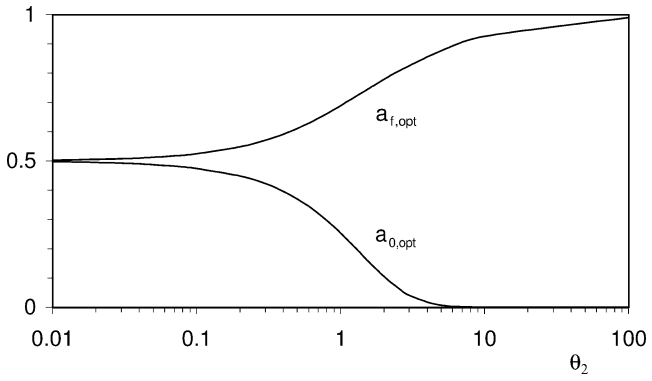

Fig. 7. The gap between the a_f and a_0 values corresponding to the optimized cycle of Fig. 4.

and the adsorption steps, respectively. Combining Eqs. (15) and (16) yields the relation between θ_1 and θ_2,

$$\theta_1 = -\ln\left(\frac{1 - a_0 \exp(\theta_2)}{1 - a_0}\right) \tag{18}$$

The time-averaged rate of A production is proportional to

$$\bar{a} = \frac{a_f - a_0}{\theta_1 + \theta_2} = \frac{a_0[\exp(\theta_2) - 1]}{\theta_2(\tau + 1)} \tag{19}$$

where τ is given by Eq. (8). Eq. (9) continues to apply, with $j_{A,\max}$ given by

$$j_{A,\max} = \frac{U_m}{d_s}(K_{Aa}C_{Aga} - K_{Ad}C_{Agd}) \tag{20}$$

Fig. 5 shows the variation of $\bar{a}$ with a_0 for several values of θ_2. This figure was constructed by combining Eqs. (18) and (19). There exists an optimal a_0 for which the average rate of A production is maximum. The optimal a_0 is equivalent to an optimal combination of parameters θ_1, τ and a_f. The maximized production rate ($\bar{a}_{\max}$) is higher when θ_2 is shorter. Solving $\partial\bar{a}/\partial a_0 = 0$ with θ_2 constant, we obtain an implicit relation between $a_{0,\text{opt}}$ and θ_2,

$$\theta_2 + \frac{a_{0,\text{opt}}[1 - \exp(\theta_2)]}{(1 - a_{0,\text{opt}})[1 - a_{0,\text{opt}}\exp(\theta_2)]} = \ln\left(\frac{1 - a_{0,\text{opt}}\exp(\theta_2)}{1 - a_{0,\text{opt}}}\right) \tag{21}$$

Combining this with Eqs. (16), (18) and (19) we obtain $a_{f,\text{opt}}$, τ_{opt} and $\bar{a}_{\max}$ as functions of θ_2. These results are reported in Figs. 6 and 7. The trends reported in Fig. 7 are similar to what we obtained based on the simpler model in Fig. 3. This time the transition from small-θ_2 behavior to large-θ_2 behavior is considerably steeper, and is located in a higher θ_2 range than in Fig. 3. As θ_2 increases, the gap widens between the a_f and a_0 values corresponding to the optimized cycle (Fig. 7).

4. Variable concentration of species A in the gas mixture

Consider now the case when the concentration of A in the gas is not fixed. During adsorption, the concentration of A in the gas mixture decreases while the concentration of A in the solid increases. The concentrations of A in solid and gas are represented by two values, C_{Ag} and C_A, which are functions of time. The concentration variation across the gas space is neglected. The C_{Ag} and C_A values are related through the species conservation statement

$$C_{Ag} - C_{Ag0} = -r(C_A - C_{A0}) \tag{22}$$

where C_{Ag0} is the initial concentration of A in the gas, and r is the ratio of the solid and gas layers thicknesses (Fig. 1).

$$r = \frac{d_s}{d} \tag{23}$$

The equilibrium concentration of A in the solid (i.e., the concentration reached when the mass transfer between gas and solid ceases) can be calculated from Eq. (22) and Henry's law at equilibrium,

$$C_{A,\text{eq}} = \frac{K_A C_{Ag0} + r K_A C_{A0}}{1 + r K_A} \tag{24}$$

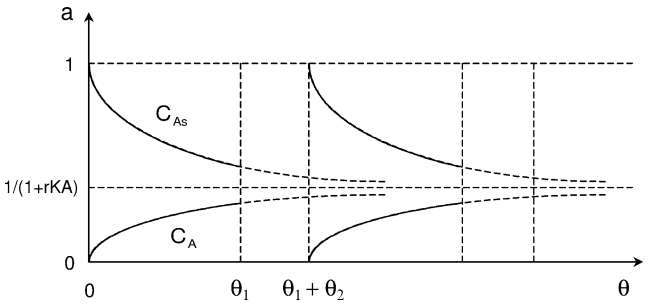

Fig. 8. Sequence of adsorption–desorption cycles with time-dependent concentration in the gas space.

From Eqs. (1)–(3) and (22) we can calculate the amount of adsorbed A,

$$a = \frac{1 - \exp[-\theta(1 + rK_A)]}{1 + rK_A} \tag{25}$$

where

$$a = \frac{C_A - C_{A0}}{K_A C_{Ag0} - C_{A0}} = \frac{C_A - C_{A0}}{(C_{A,\mathrm{eq}} - C_{A0})(1 + rK_A)} \tag{26}$$

In this formulation, parameter a takes values between 0 for $C_A = C_{A0}$, and $1/(1 + rK_A)$ for $C_A = C_{A,\mathrm{eq}}$.

Consider an adsorption–desorption cycle (Fig. 8), where the desorption mechanism is unknown but takes a fixed time θ_2. During adsorption, the concentration in the solid increases, and the concentration in the gas decreases. Both concentrations tend to the equilibrium concentration, $a = 1/(1 + rK_A)$. The time-averaged rate of A production is proportional to

$$\bar{a} = \frac{a_1}{\theta_1 + \theta_2} = \frac{1 - \exp[-\theta_1(1 + rK_A)]}{(\theta_1 + \theta_2)(1 + rK_A)} = \frac{1 - \exp[-\theta_2\tau(1 + rK_A)]}{\theta_2(\tau + 1)(1 + rK_A)} \tag{27}$$

where, according to the $\bar{a}$ definition (9), $j_{A,\max}$ is

$$j_{A,\max} = \frac{U_m}{d_s}(K_A C_{Ag0} - C_{A0}) \tag{28}$$

We find that the variation of $\bar{a}$ with τ for several values of $\theta_2(1 + rK_A)$ is the same as in Fig. 2, if θ_2 is replaced by $\theta_2(1 + rK_A)$. There exists an optimal τ (or θ_1) for which the average rate of A production is maximum. Solving $\partial\bar{a}/\partial\tau = 0$ we arrive at the equation for τ_{opt},

$$1 + \theta_2(1 + rK_A)(\tau_{\mathrm{opt}} + 1) = \exp\big(\theta_2(1 + rK_A)\tau_{\mathrm{opt}}\big) \tag{29}$$

which has the same form as Eq. (12). The corresponding τ_{opt} and $\bar{a}_{\max}$ may be viewed in Fig. 3 as functions of $\theta_2(1 + rK_A)$, if on the abscissa we replace θ_2 with $\theta_2(1 + rK_A)$. Fig. 9 shows τ_{opt} and $\bar{a}_{\max}$ as functions of θ_2 for several values of rK_A.

5. Elemental volume

In Sections 2–4 we considered the optimization of the timing of the adsorption and desorption steps. Three models

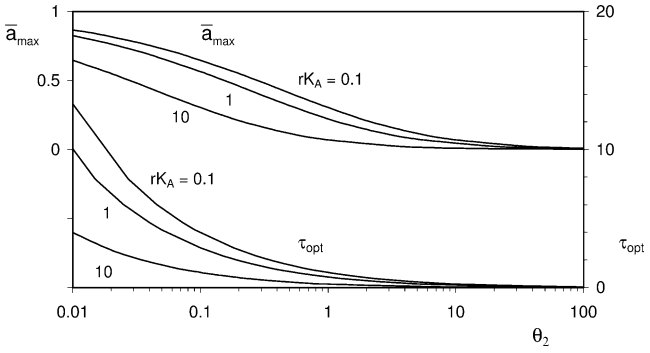

Fig. 9. The optimal time ratio and maximal adsorption rate for the model of Fig. 8.

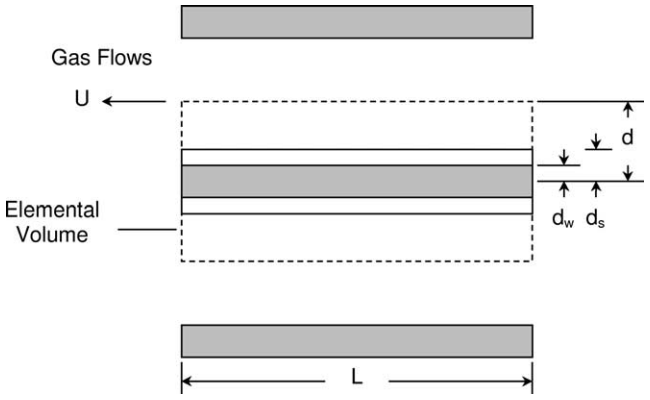

Fig. 10. Elemental volume with longitudinal gas flow and transversal diffusion length scales.

we analyzed, and each led to the conclusion that an optimal adsorption time exists when the desorption time (θ_2) is specified. In particular, Figs. 3 and 6 showed that in the limit of short desorption times ($\theta_2 \ll 1$) the optimal time ratio is $\tau = 1$, or $\theta_{1,\mathrm{opt}} = \theta_2$, and $t_{1,\mathrm{opt}} = t_2$. In this limit both time intervals are short, and, according to Eq. (10), the mass transfer rate is high. In conclusion, short and optimized times are attractive from the point of view of building high-density devices for adsorption and desorption.

In this section we explore the packing (compactness) implications of the above observation. Short times also mean small length scales. How should a macroscopic device of specified volume be filled with a large number of working channels of the type (e.g., Fig. 1) analyzed in the preceding material? Earlier constructal optimization studies have shown that optimal timing requires optimal allocation and arrangement of working material in space [1]. Temporal organization goes hand in hand with spatial organization, when the objective is to achieve the most with a device of specified size—the most per unit volume.

We pursue this objective in the direction from small to large, hierarchically, in accordance with the constructal method [1]. The start is the smallest identifiable finite-size unit that performs the intended function of adsorption and desorption. That unit is the "elemental volume" sketched in Fig. 10. For the gas volume to work best, i.e., without dead

spaces that do not participate, its transversal length scale (d) must match the length penetrated by mass diffusion during adsorption,

$$d \sim (Dt_1)^{1/2} \tag{30}$$

In this scale analysis D is the mass diffusivity of species A in the gas mixture, and "$\sim$" stands for "equal in an order of magnitude (scaling) sense" [11]. The same argument holds for the thickness of solid layer that acts as adsorbent,

$$d_s \sim (D_s t_1)^{1/2} \tag{31}$$

where D_s is the mass diffusivity of A in the solid. Finally, the same length scales must be penetrated by diffusion during the desorption step,

$$d \sim (Dt_2)^{1/2}, \qquad d_s \sim (D_s t_2)^{1/2} \tag{32}$$

Combining Eqs. (31) and (32) we arrive at the geometric requirement that the adsorption and desorption times must be of the same order of magnitude,

$$t_1 \sim t_2 \tag{33}$$

and that the transversal length scales of the elemental volume must be in a certain proportion,

$$\frac{d_s}{d} \sim \left(\frac{D_s}{D}\right)^{1/2} \tag{34}$$

Eq. (33) is the same as the equality of the two time strokes observed in respiration (inhaling, exhaling) and blood circulation (heart beating) [1]. Using $D_s \sim 10^{-10}$ m^2·s^{-1} and $D \sim 10^{-5}$ m^2·s^{-1} as representative orders of magnitude for diffusion in solid and gas, we estimate $d_s/d \sim 10^{-2}$: The layer of adsorbent that works during t_1 and t_2 is considerably thinner than the channel filled with gas. Because of mechanical strength requirements, the actual solid layer may be thicker than d_s. Alternatively, a d_s-thick layer of adsorbent may be deposited on a wall of another material of thickness d_w, which provides the needed mechanical strength.

The longitudinal length scale, or the slenderness of the elemental volume is furnished by the same requirement of squeezing the most performance out of the elemental volume. The gas channel $d \times L$ is used entirely when it is traversed by mass diffusion during the same time interval that the gas mixture resides in the channel. Said another way, during t_1 the gas flow sweeps the entire length

$$L = Ut_1 \tag{35}$$

where U is the mean velocity of the gas mixture. This means that at the channel exit the thickness of the concentration boundary layers is comparable with the diffusion length d, or that the boundary layers merge just as the gas leaves the channel.

To estimate the U scale we assume that the channel is narrow and long enough that the flow regime is laminar and fully developed,

$$U \sim \frac{d^2 \Delta P}{\mu L} \tag{36}$$

where ΔP is the pressure difference maintained in the longitudinal direction. Eq. (36) means that the entrance length for the development of the velocity profile is shorter than L. Conversely, since L is the entrance length for the development of the concentration profile, the use of Eq. (36) means that the momentum diffusivity is larger than the mass diffusivity ($\nu > D$), or that $Sc > 1$. Combining Eqs. (29), (35) and (36) we find the relation between the two dimensions of the channel,

$$\frac{L}{d^2} \sim \left(\frac{\Delta P}{\mu D}\right)^{1/2} \tag{37}$$

Eq. (37) is the mass transfer analog of the principle of packing maximum heat transfer in a given volume [1,11–14]. When the time scale t_1 (or t_2) decreases, the transversal length scale (d) decreases as $t_1^{1/2}$, and the longitudinal scale decreases as t_1, i.e., faster than d. We can always imagine a t_1 scale so small that the calculated L is smaller than d: such a case violates the slender channel assumption that served as basis for the boundary layer and Hagen–Poiseuille flow assumptions made earlier in this analysis. Consequently, we invoke the channel slenderness constraint $L/d > 1$, which in combination with Eqs. (37) and (29) yields the following criteria for the validity of this analysis:

$$d > \left(\frac{\mu D}{\Delta P}\right)^{1/2} \tag{38}$$

$$t_1 > \frac{\mu}{\Delta P} \tag{39}$$

In summary, when the time scale t_1 (or t_2) is specified, all the dimensions of the elemental volume can be calculated from the requirement that the entire elemental volume must be used with purpose: to adsorb and desorb the species of interest. How well is the optimized elemental geometry performing? In other words, what quantity of species A is being removed from the gas mixture per unit volume and per unit time? We answer by continuing to assume that the geometry is two-dimensional, i.e., the elemental volume is represented by the area $L \times d$, when the d scale is greater than $(d_s + d_w)$. The quantity of interest is related to the mass flux scale associated with the time scale t_1,

$$j_A \sim D\frac{\Delta C}{d} \sim \Delta C\left(\frac{D}{t_1}\right)^{1/2} \tag{40}$$

where ΔC is the scale of the concentration difference, e.g., $C_{As} - C_A$ in Eq. (1). The total amount of A removed from the gas mixture by one elemental volume during one cycle is of order $j_A L t_1$. The units of the group $j_A L t_1$ are kmol·m^{-1}, that is the amount of A per unit of length perpendicular to the $L \times d$ plane. The rate of A removal per unit volume and per unit time is $\dot{n}''' = (j_A L t_1)/(L d t_1)$, or

$$\dot{n}''' \sim D\frac{\Delta C}{d^2} \sim \frac{\Delta C}{t_1} \tag{41}$$

This quantity increases sharply as t_1 decreases. The largest $\dot{n}'''$ that can be estimated based on this slender-channel formulation is obtained by combining Eq. (41) with Eq. (39),

$$\dot{n}''' < \frac{\Delta C \Delta P}{\mu} \tag{42}$$

The $\dot{n}'''$ estimate of Eq. (41) can also be derived from the conservation of species argument. The cycle-averaged rate at which species A is brought into the elemental volume by the gas mixture, $\Delta C U d$, must be the same as the rate at which the elemental volume removes species A from the mixture, $\dot{n}''' L d$. This balance means

$$\dot{n}''' \sim \Delta C \frac{U}{L} \tag{43}$$

which, after using the U and L scales derived earlier, leads to Eq. (41).

6. First construct

In this and the following sections we show that there is an optimal number of elemental volumes that must be grouped together, so that the power required to pump the gas mixture is minimum. The construction sequence leads to tree-shaped flow structures of the hierarchical type that have been constructed for heat flow and fluid flow [9,10, 14]. The elemental scales developed in Eqs. (29)–(43) show that the geometry of the elemental volume has two degrees of freedom, which are represented by d and L, or by the independent parameters t_1 and ΔP. For the sake of clarity, let us assume that the time scale t_1 is fixed on the basis of a specified (desired) volumetric density of A production, $\dot{n}'''$, cf. Eq. (41). In this case the transversal length scale d is fixed, while L increases as $\Delta P^{1/2}$, cf. Eq. (37). The size of the elemental volume (Ld) also increases as $\Delta P^{1/2}$.

Consider now the 'first construct' shown in Fig. 11, where n_1 elemental volumes are stacked and bathed in parallel by the total gas mixture stream $\dot{m}'_1$ [kg·s·m^{-1}]. The global size of the first construct (A_1) is fixed, $A_1 \sim L L_1$, where L_1 is the total thickness of the stack, $L_1 \sim n_1 d$. In conclusion, the A_1 size constraint reads

$$A_1 \sim n_1 d L \tag{44}$$

in which n_1 and L may vary. The overall mass flow rate $\dot{m}'_1$ is fixed because $A_1, \dot{n}'''$ and the overall rate of species production ($\dot{n}'''\ A_1$) are fixed. The pumping power that is required to drive $\dot{m}'_1$ through the construct is proportional to $\dot{m}'_1$ times the overall pressure drop between the inlet and the outlet of the $\dot{m}'$ stream. The overall pressure drop has two terms, $\Delta P_1 = \Delta P + \Delta P_{L1}$, and ΔP_{L1} is due to the flow in the L_1 direction, which supplies each element. This second pressure drop can be estimated in an order of magnitude sense by assuming again fully developed laminar flow, cf. Eq. (36) and Fig. 11,

$$U_1 \sim \frac{d_1^2 \Delta P_{L1}}{\mu L_1} \tag{45}$$

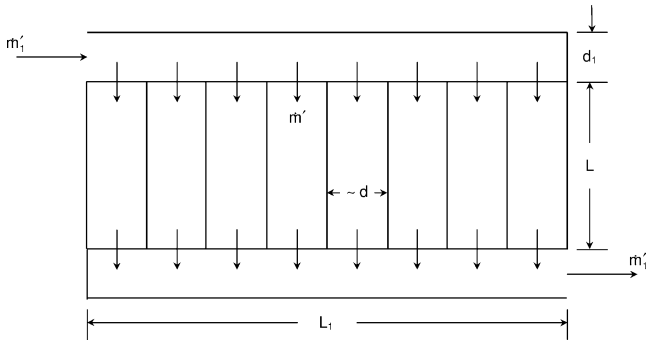

Fig. 11. First construct containing a large number of elemental volumes supplied by a single stream.

where $U_1 \sim \dot{m}'_1/(\rho d_1)$. We assume that the spacing d_1 scales with, and is a small fraction of the thickness of the entire construct,

$$\frac{d_1}{L} = \phi_1 \ll 1 \tag{46}$$

The length of the construct is

$$L_1 \sim n_1 d \tag{47}$$

To minimize the overall pumping power when the flow rate $\dot{m}'$ is fixed, is the same as minimizing the total pressure drop. After using the geometric relations listed for A_1, d_1 and L_1, the total pressure drop assumes the form

$$\Delta P_1 = \Delta P + \Delta P_{L1} \sim \dot{m}'_1 \nu \left[\frac{A_1/d^2}{(n_1 d)^2} + \frac{(n_1 d)^4}{(\phi_1 A_1)^3} \right] \tag{48}$$

This expression shows the tradeoff role played by the number of elements in the assembly. The pressure drop is minimum when the two terms in the square brackets are of the same order of magnitude, and this occurs when

$$n_{1,\mathrm{opt}} \sim \left(\frac{A_1}{d^2} \right)^{2/3} \phi_1^{1/2} \tag{49}$$

At this optimum, the slenderness of the elemental volume is

$$\frac{L}{d} \sim \left(\frac{A_1}{d^2} \right)^{1/3} \phi_1^{-1/2} \gg 1 \tag{50}$$

The inequality sign is a reminder that the elemental volume was assumed to be slender, which is consistent with the geometric fact that $A_1 \gg d^2$, and with the assumption that $\phi_1 \ll 1$. The corresponding aspect ratio of the first construct is

$$\frac{L_1}{L} \sim \left(\frac{A_1}{d^2} \right)^{1/3} \phi_1 \tag{51}$$

Eq. (51) shows that the group $(A_1/d^2)^{1/3}$ controls this aspect ratio, as it did at the elemental level, Eq. (50). The difference is the effect of $\phi_1 (\ll 1)$, which makes the elemental volume more slender than the first construct.

The overall pressure drop that is minimum when Eq. (49) holds is of order

$$\Delta P_1 \sim \frac{\dot{m}'_1 \nu}{d^2 \phi_1} \left(\frac{A_1}{d^2} \right)^{-1/3} \tag{52}$$

Because $\dot{m}'_1$ scales as $\dot{m}'''A_1$, where the volumetric flow rate must be proportional to $\dot{n}'''$, the overall pressure drop increases as $A_1^{2/3}$ as the overall size of the first construct increases. In other words, the overall pressure drop increases in direct proportion with n_1, cf., Eq. (49). The overall pumping power required by the first construct is

$$\dot{W}'_1 \sim (\dot{m}''')^2 \frac{\nu d^2}{\rho \phi_1} \left(\frac{A_1}{d^2}\right)^{5/3} \tag{53}$$

The proportionality between $\dot{W}'_1$ and $A_1^{5/3}$ means that larger first constructs require more power, and that the rate of power increase increases with A_1. The question investigated in the next section is whether it might be possible to slow down this trend, perhaps by using a flow configuration that differs from the choice made in Fig. 11.

7. Second construct

Consider next the 'second construct' flow configuration shown in Fig. 12. The size of this flow system is $A_2 = L_1 L_2 = n_2 A_1$, where n_2 is the number of first constructs of the type shown in Fig. 11. In the following analysis we assume that all the geometric features of each A_1 construct have been optimized as shown in the preceding section. The total flow rate $\dot{m}'_2$ is proportional to the overall size, $\dot{m}'_2 = \dot{m}'''A_2$, so that the specified volumetric flow rate $\dot{m}'''$ (or $\dot{n}'''$) is respected.

The overall pressure drop experienced by $\dot{m}'_2$ is $\Delta P_2 = \Delta P_1 + \Delta P_{L2}$, where ΔP_{L2} is the scale of the pressure drop along the channels of length L_2 and spacing d_2. We assume again that d_2 is a certain (small) fraction of the overall dimension of the construct,

$$\frac{d_2}{L_1} = \phi_2 \ll 1 \tag{54}$$

It can be shown that the total pressure drop can be written as

$$\begin{aligned}\Delta P_2 &\sim \dot{m}'_2 \nu \left[\frac{n_2 L}{\phi_2^3 L_1^3} + \frac{(d^2/A_1)^{1/3}}{n_2 d^2 \phi_1}\right] \\ &\sim \dot{m}'_2 \nu \left[\frac{n_2^{8/3}}{\phi_1 \phi_2^3 d^2}\left(\frac{d^2}{A_2}\right)^{5/3} + \frac{1}{n_2^{2/3} d^2 \phi_1}\left(\frac{d^2}{A_2}\right)^{1/3}\right]\end{aligned} \tag{55}$$

The optimal number of constituents for which ΔP_2 is minimum is

$$n_{2,\mathrm{opt}} \sim \phi_1^{3/10} \phi_2^{9/10} \left(\frac{A_2}{d^2}\right)^{2/5} \tag{56}$$

The corresponding aspect ratio, overall pressure drop, and pumping power are

$$\frac{L_2}{L_1} \sim \phi_1^{-3/5} \phi_2^{6/5} \left(\frac{A_2}{d^2}\right)^{1/5} \tag{57}$$

$$\Delta P_2 \sim \frac{\dot{m}'_2 \nu}{d^2 \phi_1^{6/5} \phi_2^{3/5}} \left(\frac{A_2}{d^2}\right)^{-3/5} \tag{58}$$

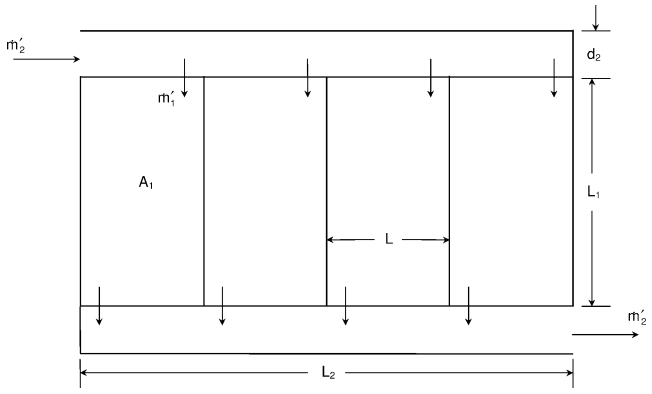

Fig. 12. Second construct containing a large number of first constructs supplied by a single stream.

$$\dot{W}'_2 \sim \frac{(\dot{m}''')^2 \nu d^2}{\rho \phi_1^{6/5} \phi_2^{3/5}} \left(\frac{A_2}{d^2}\right)^{7/5} \tag{59}$$

Eqs. (56)–(59) should be examined on the background offered by the corresponding results obtained for the first-construct configuration, Eqs. (49)–(53). Although the relations are similar, the differences are the important features, i.e., the basis on which the designer may choose between using a first construct or a second construct. The most important feature is that the pumping power required by the second construct increases as $A_2^{7/5}$, which is a slower rate of increase than in the case of the first construct, Eq. (53).

If we were to plot Eqs. (53) and (59) as the power required ($\dot{W}'_{1,2}$) versus the overall size ($A_{1,2}$), we would see that the two curves intersect. Let $A_{1-2} = A_1 = A_2$ represent the critical system size where $\dot{W}'_1 = \dot{W}'_2$. We choose between the configurations of Figs. 11 and 12 so that the required pumping power is the smaller of $\dot{W}'_1$ and $\dot{W}'_2$. We find that when the system size is smaller than A_{1-2}, the better configuration is the first construct. When the size is greater than A_{1-2}, the preferred configuration is the second construct. In this way we discover the *transition* from the first-construct flow pattern to the second-construct flow pattern. This transition is analogous to other flow pattern transitions covered by constructal theory, e.g., laminar-turbulent flow, and Bénard convection [1]. In the present case, the intersection of Eqs. (53) and (59) yields

$$\frac{A_{1-2}}{d^2} \sim \phi_1^{-3/4} \phi_2^{-9/4} \gg 1 \tag{60}$$

The optimized second construct is less slender than the optimized first construct of the same size. Compare Eq. (51) with Eq. (57), and assume that $A_1 = A_2$ and $\phi_1 = \phi_2 = \phi$. The first-construct slenderness is proportional to ϕ, while the second-construct slenderness is proportional to $\phi^{3/5}$, which is larger than ϕ because ϕ is much smaller than 1. Optimized constructs become less slender, more square like, as their size and complexity increase.

8. Higher-order constructs

The construction and optimization sequence that we started in Figs. 10–12 can be continued toward more complex (compounded) flow structures that cover larger spaces. At each new level of assembly, the analysis follows the steps outlined in the preceding two sections. Here we report only the final results for the third construct, which is defined in Fig. 13.

This configuration is represented by $A_3 = L_2L_3$, $d_3/L_2 = \phi_3 \ll 1$, $\dot{m}'_3 = n_3\dot{m}'_2$, $A_3 = n_3A_2$, and $L_3 = n_3L_1$, where n_3 is the number of second-order constructs assembled into the third-order construct. The flow architecture for which the overall pressure drop and pumping power are minimized is represented by

$$n_{3,\text{opt}} \sim \phi_1^{-9/14}\phi_2^{9/14}\phi_3^{15/14}\left(\frac{A_3}{d^2}\right)^{2/7} \tag{61}$$

$$\frac{L_3}{L_2} \sim \phi_1^{-3/7}\phi_2^{-3/7}\phi_3^{9/7}\left(\frac{A_3}{d^2}\right)^{1/7} \tag{62}$$

$$\Delta P_3 \sim \frac{\dot{m}'_3\nu}{d^2\phi_1^{6/7}\phi_2^{6/7}\phi_3^{3/7}}\left(\frac{A_3}{d^2}\right)^{-5/7} \tag{63}$$

$$\dot{W}'_3 \sim \frac{(\dot{m}''')^2\nu d^2}{\rho\phi_1^{6/7}\phi_2^{6/7}\phi_3^{3/7}}\left(\frac{A_3}{d^2}\right)^{9/7} \tag{64}$$

Eqs. (61)–(64) can be compared with the corresponding results obtained for the optimized second construct, Eqs. (56)–(59), to see when it is beneficial to change the flow structure, from Figs. 12 and 13. Note that the third-construct power requirement (64) increases more slowly with the size of the construct than in Eq. (59). Consequently, by intersecting the curves (59) and (64) we find the transition size A_{2-3} where $A_2 = A_3$ and $\dot{W}'_2 = \dot{W}'_3$,

$$\frac{A_{2-3}}{d^2} \sim \phi_1^3\phi_2^{-9/4}\phi_3^{-15/4} \tag{65}$$

In the sequence started by Eqs. (53), (59) and (64), $\dot{W}'$ is proportional to A^m, where the exponent m decreases as the series $5/3, 7/5, 9/7, 11/9, 13/11, \ldots$. This suggests that in sufficiently complex and large constructs, m approaches 1, and $\dot{W}'$ is proportional to the size A.

The distribution of the channel volume fractions over the many scales that are present in the dendritic flow structure $(\phi_1, \phi_2, \phi_3, \ldots)$ can be optimized further, with the objective of minimizing the overall pumping power requirement. For example, Eq. (59) shows that $\dot{W}'_2$ can be minimized by maximizing $\phi_1^{6/5}\phi_2^{3/5}$, which is equivalent to maximizing the group $\phi_1^2\phi_2$. The fractions ϕ_1 and ϕ_2 are related through the overall channel volume constraint

$$\frac{A_{2,\text{channels}}}{A_2} = \frac{2d_2L_2 + n_2d_1L_1}{A_2} \tag{66}$$

or

$$\phi_{12} = 2\phi_2 + \phi_1 \tag{67}$$

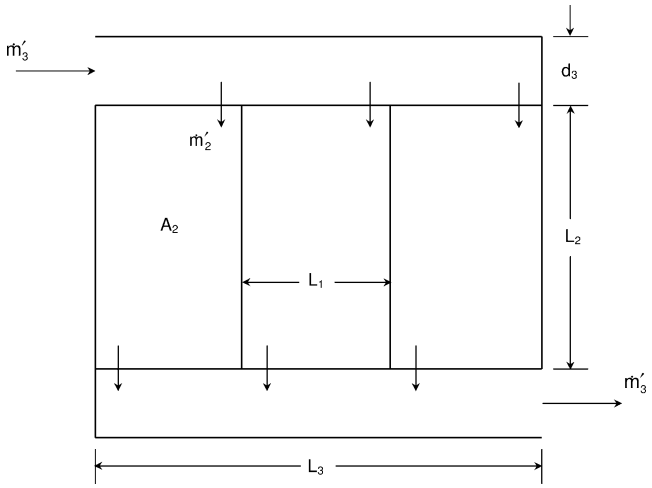

Fig. 13. Third construct containing a large number of second constructs supplied by a single stream.

where ϕ_{12} $(= A_{2,\text{channels}}/A_2)$ is the fixed volume fraction occupied by all the channels present inside A_2. The maximization of $\phi_1^2\phi_2$ subject to constraint (67) yields $\phi_1 = 2\phi_{12}/3$, $\phi_2 = \phi_{12}/4$, and a minimized $\dot{W}'_2$ value that is proportional to $(\phi_{12}/3)^{-9/5}$.

At the second construct level, Eq. (64) shows that $\dot{W}'_3$ can be minimized by maximizing the product $(\phi_1\phi_2)^{6/7}\phi_3^{3/7}$, which according to the preceding paragraph is proportional to $(\phi_{12}^2)^{6/7}\phi_3^{3/7}$. The objective then is to maximize the group $\phi_{12}^4\phi_3$ subject to the total channel volume constraint,

$$\phi_{13} = 2\phi_3 + \phi_{12} \tag{68}$$

where ϕ_{13} $(= A_{3,\text{channels}}/A_3)$ is the volume fraction occupied by all the channels in the third construct. The maximization of $\phi_{12}^4\phi_3$ subject to constraint (68) yields $\phi_3 = \phi_{13}/10$, $\phi_{12} = 4\phi_{13}/5$, and a $\dot{W}'_3$ value proportional to $(\phi_{13}/1.895)^{-15/7}$. Inside each of the second constructs present in A_3, the overall channel volume is distributed in accordance with the distribution of ϕ_{12}, namely, $\phi_1 = (2/3)\phi_{12} = (8/15)\phi_{13}$, and $\phi_2 = (1/4)\phi_{12} = (1/5)\phi_{13}$. In summary, the 'internal' volume fractions decrease $(\phi_1 > \phi_2 > \phi_3 > \cdots)$ as the length scale of each new channel increases.

Another way to summarize the optimization of channel volume distribution is to note that starting with Eq. (53) the pumping power $(\dot{W}'_1, \dot{W}'_2, \dot{W}'_3, \ldots)$ is proportional to $\phi_1^{-1}, \phi_{12}^{-9/5}, \phi_{13}^{-15/7}, \ldots$. In this sequence, ϕ_1, ϕ_{12} and ϕ_{13} represent the overall channel volume fraction of the construct. The exponents $-1, -9/5, -15/7, \ldots$ suggest the sequence $-3/3, -3 \times 3/5, -3 \times 5/7, -3 \times 7/9, -3 \times 9/11, \ldots$, which shows how the overall channel volume fraction affects the overall pumping power requirement.

The external aspect ratios of the flow structures decrease as the constructs become larger and more complex. The aspect ratios of Eqs. (51), (57) and (62) are summarized by

$$\frac{L_i}{L_{i-1}} \sim \phi^p\left(\frac{A}{d^2}\right)^q \tag{69}$$

where the exponents decrease ($p = 1, 3/5, 9/35, \ldots$; $q = 1/3, 1/5, 1/7, \ldots$) as the order of the construct (i) increases. This means that the external shape of the flow structure approaches a square as the size and order of the design increase.

9. Conclusions

In this paper we used simple modeling and analysis to show how adsorption processes can be optimized in time and space. In the first part of the paper, we used several models to show that the periodicity of an adsorption process can be optimized. For example, when the desorption time is fixed, the time interval allocated to adsorption can be optimized as shown in Fig. 2. More general versions of this optimization opportunity are presented in Fig. 6 for processes with variable desorption times, and in Fig. 9 for processes with variable concentration in the gas space.

In each case, the demonstration was based on the simplest possible model for the sake of simplicity. The modeling was focused mainly on the adsorption phase. To describe the desorption phase we used a group of global parameters such as the time interval θ_2, which was allowed to vary in the more general model of Section 3. Future studies may reconsider the time-optimization opportunity by modeling the entire cycle of adsorption and desorption, i.e., by accounting for the coupling between the two phases of the cycle. The main reason for using the simplest model first is also the main conclusion: there exist opportunities to optimize the periodicity of size-constrained mass transfer devices.

In the second part of the paper, we built the small-scale spatial structure of the adsorption system based on the time scales of the associated diffusion processes (Section 5). The basic idea is to use all the available space [1] for the purpose of housing mass diffusion. This led to the elemental channel with the L/d^2 ratio given by Eq. (37): maximum volumetric density of mass transfer is achieved when each elemental channel is as long as the mass transfer entrance length of laminar flow. The elemental channels were grouped optimally into first constructs (Section 6), second constructs (Section 7), and constructs of higher order (Section 8). We showed that at each level of construction the optimization of architecture is achieved by selecting the number of constituents and the distribution of available void (channel) space among all the channels. The construction objective is to pack the available space with elemental channels in such a way that the overall pumping power is minimal. The optimized architectures arrange themselves in a sequence that can be extended (by inspection) to higher orders of construction, as shown at the end of Section 8. The flow architecture is that of two fluid trees matched canopy to canopy: this structure was proposed first for compact heat transfer devices [1,9,10,14].

The main conclusion of this work is that optimization opportunities for temporal and spatial structure exist, and that they deserve to be pursued in the quest for mass exchangers with maximal concentration of mass per unit volume. To cover this fundamental territory, we used the simplest models. Future studies may consider these issues based on more complex and more realistic models. The fundamental aspect of the time and space tradeoffs identified in this paper assures us that similar tradeoffs will rule optimization in more refined descriptions of adsorption-desorption processes.

Another expected trend is that of increasing robustness as the complexity of the flow structure increases [1]: complex structures tend to exhibit near-optimal performance even though they may not match in every detail the geometry of the ultimate (optimal) design. This trend makes the constructal sequence (Sections 5–8) a valuable and direct path to designs that are complex and sufficiently optimized to operate at near-optimal levels. Future work may also search for improvements in the constructal method, for example, more direct (analytical) strategies for the optimal structure. One recent development is the proposal to minimize flow path lengths [15] instead of minimizing fluid flow resistance at every level of assembly [16]. A comparison between the two methods [15,16] shows that the minimization of flow path lengths is considerably more direct and surprisingly accurate. This lends even more support to the view that optimized dendritic flow structures are robust, and that many classes of near-optimal designs perform nearly as well as the optimal design.

Acknowledgement

The research reported in this paper was supported by a grant from the National Science Foundation.

References

[1] A. Bejan, Shape and Structure, from Engineering to Nature, Cambridge University Press, Cambridge, 2000.
[2] D.M. Ruthven, S. Farooq, K.S. Knaebel, Pressure Swing Adsorption, VCH Publishers, New York, 1994.
[3] D.M. Ruthven, Principles of Adsorption and Adsorption Processes, Wiley, New York, 1984.
[4] K.S. Knaebel, F.B. Hill, Pressure swing adsorption: development of an equilibrium theory for gas separations, Chem. Engrg. Sci. 40 (1985) 2351–2360.
[5] R. Banerjee, K.G. Narayankhedkar, S.P. Sukhatme, Exergy analysis of pressure swing adsorption processes for air separation, Chem. Engrg. Sci. 45 (1990) 467–475.
[6] N.S. Raghavan, D.M. Ruthven, Pressure swing adsorption. Part III: Numerical simulation of a kinetically controlled bulk gas separation, AIChE J. 31 (1985) 2017–2025.
[7] R. Banerjee, K.G. Narayankhedkar, S.P. Sukhatme, Exergy analysis of kinetic pressure swing adsorption processes: comparison of different cycle configurations, Chem. Engrg. Sci. 47 (1992) 1307–1311.
[8] M.M. Hassan, D.M. Ruthven, N.S. Raghavan, Air separation by pressure swing adsorption on a carbon molecular sieve, Chem. Engrg. Sci. 41 (1986) 1333–1343.

[9] A. Bejan, Dendritic constructal heat exchanger with small-scale crossflows and larger-scales counterflows, Internat. J. Heat Mass Transfer 45 (2002) 4607–4620.
[10] A. Bejan, The tree of convective heat streams: Its thermal insulation function and the predicted 3/4-power relation between body heat loss and body size, Internat. J. Heat Mass Transfer 44 (2001) 699–704.
[11] A. Bejan, Convection Heat Transfer, 2nd Edition, Wiley, New York, 1995.
[12] A. Bejan, E. Sciubba, The optimal spacing of parallel plates cooled by forced convection, Internat. J. Heat Mass Transfer 35 (1992) 3259–3264.
[13] L.A.O. Rocha, A. Bejan, Geometric optimization of periodic flow and heat transfer in a volume cooled by parallel tubes, J. Heat Transfer 123 (2001) 233–239.
[14] A. Bejan, M.R. Errera, Convective trees of fluid channels for volumetric cooling, Internat. J. Heat Mass Transfer 43 (2000) 3105–3118.
[15] S. Lorente, W. Wechsatol, A. Bejan, Tree shaped flow structures designed by minimizing path lengths, Internat. J. Heat Mass Transfer 45 (2002) 3299–3312.
[16] W. Wechsatol, S. Lorente, A. Bejan, Optimal tree-shaped networks for fluid flow in a disc-shaped body, Internat. J. Heat Mass Transfer 45 (2002) 4911–4924.